16

A Dual-Frequency Metallic Waveguide System

Yoshihiro Kokubo
Graduate School of Engineering, University of Hyogo, Himeji-shi, Hyogo
Japan

1. Introduction

Conventional metallic waveguides have several major advantages, including low propagation losses and high power transmissions in the microwave frequency range. One disadvantage of metallic waveguides is that the propagation frequency band is limited at frequencies above the cutoff frequency f_c. The usable frequency range is therefore restricted to $f_c < f < 2f_c$, because the TE_{20} mode can exist in rectangular metallic waveguides at frequencies higher than $2f_c$. A ridge waveguide (or a double-ridge waveguide) (Cohn, 1947) has the advantage that it can extend the propagating frequency range by reducing the cutoff frequency for the TE_{10} mode. However, it has disadvantages in that it has a small and complex structure and a high attenuation constant.

We investigated a new type of waveguide in which single-mode propagation is possible at frequencies higher than $2f_c$ using two arrays of dielectric rods with a dielectric constant of between 20 and 30 (Shibano et al., 2006 ; Kokubo et al., 2007a).

This chapter introduces a system that uses a dual-frequency band waveguide. Firstly, we present the fundamental principles of this dual-frequency band waveguide in which a dual in-line dielectric array is installed. Since the electromagnetic reflection coefficient of a periodic array of dielectric rods is frequency dependent, at low frequencies electromagnetic waves may pass through the dual in-line dielectric rods located near the sidewalls, while at high frequencies electromagnetic waves may be reflected between them. Higher modes are suppressed in the waveguide when the space between two dielectric arrays is narrower than the space between the metal sidewalls.

Secondly, if this type of waveguide contains a corner bend and a straight portion with even symmetry (including the power source), then the dielectric rods are only required in the corner bends of the waveguide, because odd-symmetry modes (such as TE_{20}) are not excited (Kokubo et al., 2007b). As an example, a 90° bend waveguide is considered and its S-parameters are calculated. Another thick dielectric rod is located at the boundary between regions with and without dielectric rods, as reflection occurs there. This dielectric rod functions as a dielectric lens, concentrating electromagnetic waves at the center of the waveguide.

Thirdly, we introduce a frequency multiplexer or demultiplexer that mixes or separates electromagnetic waves with wide band frequencies (Kokubo & Kawai, 2008). A coaxial waveguide converter is usually used for introducing electromagnetic waves into a waveguide. However, there is no converter that can match the impedance over such a wide

frequency range. Accordingly, two converters for required for low and high frequency ranges, and electromagnetic waves must be separated into these two frequency ranges using a frequency demultiplexer.
Finally, the rods must span the entire waveguide without any gaps at the top or bottom which presents problems for fabrication. To overcome these problems, holes with diameters slightly larger than the rods were fabricated at the top of the waveguide and the dielectric rods were inserted into these holes.

2. Structure of dual-frequency waveguide and calculation method

Since the electromagnetic reflection coefficient of the imaginary wall shown in Fig. 1 is frequency dependent, at low frequencies electromagnetic waves may pass through the two imaginary walls located near the sidewalls, while at high frequencies electromagnetic waves may be reflected between them. Higher modes are suppressed in the waveguide as the space between two imaginary walls is narrower than the space between the metal sidewalls. This type of imaginary wall can be realized by an array of dielectric rods. The transmittance of electromagnetic waves for a single row of dielectric rods as a function of frequency is shown in Fig. 2 for four different incident angles. The transmittance is calculated using the cylindrical wave expansion method (Maradudin & McGurn, 1993 ; Tayeb & Maystre, 1997). The dielectric rods are assumed to be made of $LaAlO_3$ (dielectric constant $\varepsilon_r = 24$) and their radius is $r = 0.09a$, where a is the spatial period of the rods, and the electric field is parallel to the rod axes. The transmittance of electromagnetic waves is high at low frequencies ($\omega a/2\pi c \approx 0.2$) and is low at high frequencies ($\omega a/2\pi c \approx 0.45$), although it varies depending on the incident angle. An array of dielectric rods can function as an imaginary wall.

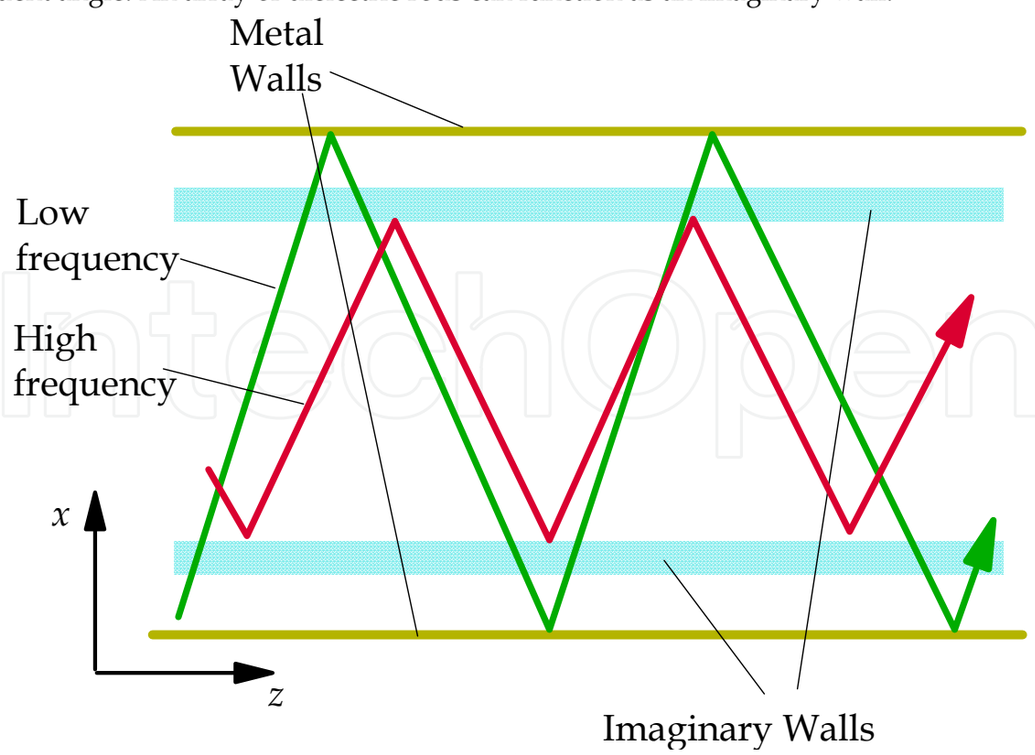

Fig. 1. Imaginary walls in a metallic waveguide.

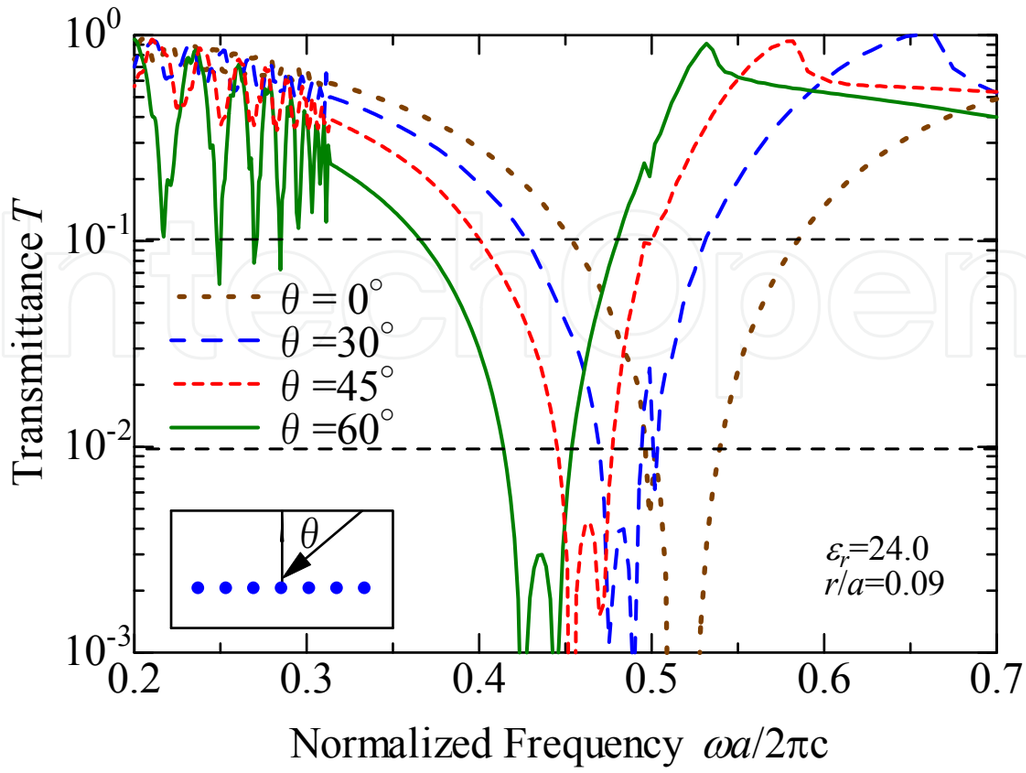

Fig. 2. Transmittance of electromagnetic waves for a single row of dielectric rods for four different incident angles between 0 and 60 degrees for ε_r=24 and r/a=0.09.

The propagation modes in this waveguide differ from those in conventional metallic waveguides. They can be calculated by the supercell approach (Benisty, 1996) by applying appropriate periodic Bloch conditions at the boundary of the unit cell (Boroditsky et al., 1998). Fig. 3(a) shows the detailed profile of the waveguide with dielectric arrays. The computational domain (super cell) shown in Fig. 3(b) is excited by a modulated Gaussian pulse and observed somewhere within the unit cell. Such observation points are located out of symmetry planes for the lattice to avoid the possibility of probing a null value of the possible propagation modes. The circumference of the unit cell is terminated by applying Bloch boundary conditions at the lateral surfaces $z = \pm a/2$, $x = 0$, and $x = w_1$. At $x = 0$ and $x = w_1$, however, boundary conditions are employed that enforce the electric walls. Maxwell's equations are solved and the field is determined at various points in the computational domain for each value of the wave vector **k**, which is normally selected along the edges of the Brillouin zone. The Fourier transform of the computed signal has peaks at frequencies of modes that can propagate in the structure for a given value of the wave vector **k**.
In fact, the periodic boundary conditions include the wave vector **k**, and can be expressed in the frequency domain as:

$$\mathbf{E}(\mathbf{r}+\mathbf{R};t) = \mathbf{E}(\mathbf{r};t)\cdot\exp(j\mathbf{k}\cdot\mathbf{R}) \tag{1}$$

$$\mathbf{H}(\mathbf{r}+\mathbf{R};t) = \mathbf{H}(\mathbf{r};t)\cdot\exp(j\mathbf{k}\cdot\mathbf{R}) \tag{2}$$

where **R** represents a lattice constant vector.

The above equations may be implemented in the time domain in several ways, but to achieve stable results it is convenient to introduce two electromagnetic fields, with time dependences sin(ωt) and cos(ωt), denoted by [$\mathbf{e}_1(\mathbf{r};t)$, $\mathbf{h}_1(\mathbf{r};t)$] and [$\mathbf{e}_2(\mathbf{r};t)$, $\mathbf{h}_2(\mathbf{r};t)$], respectively.(Boroditsky et al., 1998)

$$\mathbf{E}(\mathbf{r};t) = \mathbf{e}_1(\mathbf{r};t) + j\mathbf{e}_2(\mathbf{r};t) \tag{3}$$

$$\mathbf{H}(\mathbf{r};t) = \mathbf{h}_1(\mathbf{r};t) + j\mathbf{h}_2(\mathbf{r};t) \tag{4}$$

The periodic boundary conditions in equations (1) and (2) may then be written in the time domain as:

$$\mathbf{e}_1(\mathbf{r}+\mathbf{R};t)\cdot = \mathbf{e}_1(\mathbf{r};t)\cdot\cos(\mathbf{k}\cdot\mathbf{R}) - \mathbf{e}_2(\mathbf{r};t)\cdot\sin(\mathbf{k}\cdot\mathbf{R}) \tag{5}$$

$$\mathbf{e}_2(\mathbf{r}+\mathbf{R};t)\cdot = \mathbf{e}_1(\mathbf{r};t)\cdot\sin(\mathbf{k}\cdot\mathbf{R}) + \mathbf{e}_2(\mathbf{r};t)\cdot\cos(\mathbf{k}\cdot\mathbf{R}) \tag{6}$$

$$\mathbf{e}_1(\mathbf{r};t)\cdot = \mathbf{e}_1(\mathbf{r}+\mathbf{R};t)\cdot\cos(\mathbf{k}\cdot\mathbf{R}) + \mathbf{e}_2(\mathbf{r}+\mathbf{R};t)\cdot\sin(\mathbf{k}\cdot\mathbf{R}) \tag{7}$$

$$\mathbf{e}_2(\mathbf{r};t)\cdot = -\mathbf{e}_1(\mathbf{r}+\mathbf{R};t)\cdot\sin(\mathbf{k}\cdot\mathbf{R}) + \mathbf{e}_2(\mathbf{r}+\mathbf{R};t)\cdot\cos(\mathbf{k}\cdot\mathbf{R}) \tag{8}$$

These relations, together with analogous ones for the magnetic field, allow the field to be updated at the periodic boundaries of the computational domain. It is worth emphasizing that equations (5-8) introduce the direction of propagation and the value of the phase constant into the computations (Boroditsky et al., 1998).

The calculated results for r = 0.09a, w_1 = 2.5a, and w_2 = 1.8a are shown in Fig. 4, where w_1 is the width of the waveguide and w_2 is the distance between two dielectric arrays. If the rectangular waveguide is a WR-90 waveguide (22.9 × 10.2 mm; $f_c \approx$ 6.55 GHz), a is determined from $w_1/2.5$ = 9.16 mm. As expected, a single mode is available between 5.93 and 9.26 GHz, and between 12.33 and 17.55 GHz.

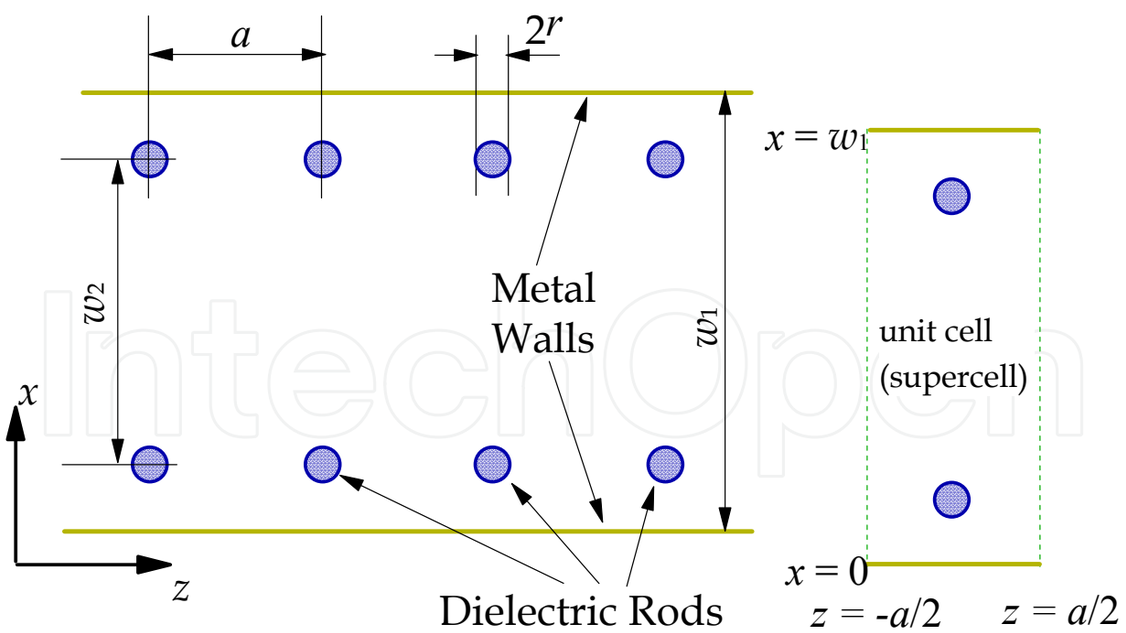

Fig. 3 (a) Detailed profile of the dual band waveguide. (b) Computational domain in real space for the calculating of the dispersion diagram.

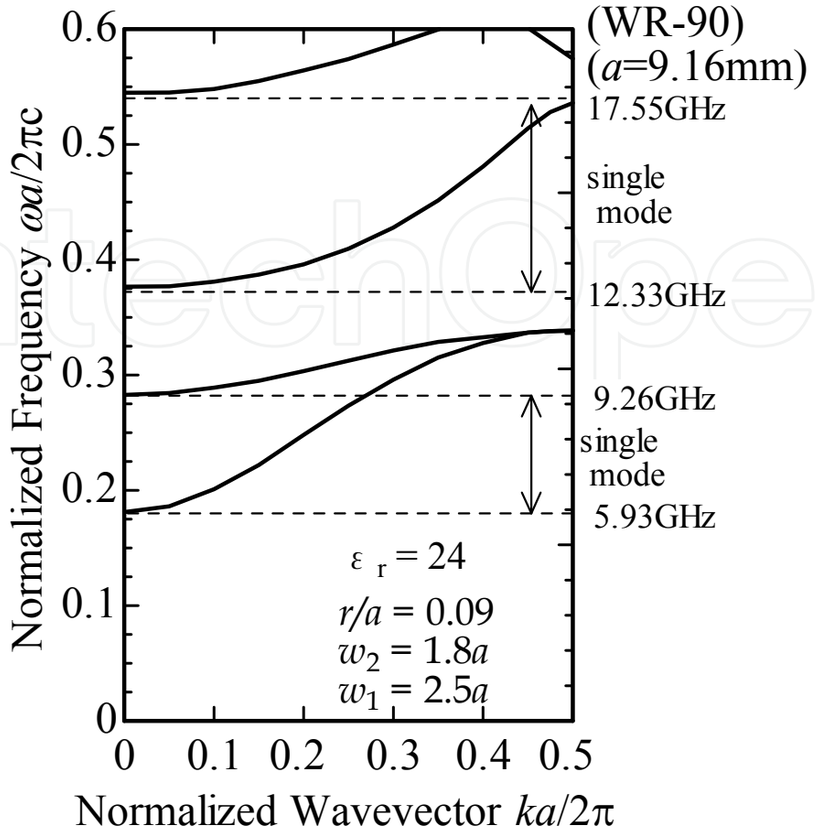

Fig. 4 Eigenvalue dispersion along the guide axis.

3. 90-degree bend waveguide

If this type of waveguide contains a corner bend and a straight portion with even symmetry (including the power source), then dielectric rods are only required in the corner bend of the waveguide, because odd-symmetry modes (such as TE_{20}) are not excited (Kokubo et al., 2007b). The proposed waveguide structure does not have dielectric rods in the straight portion; rather it has them only in the corner bend, as shown in Fig. 5(a). Firstly, the reflection coefficients $|S_{11}|$ are calculated using HFSS (Ansoft Corporation, 2005). Secondly, a scheme for reducing the reflection coefficients is proposed.

The metallic waveguide is assumed to be a WR-90 waveguide (22.9×10.2 mm, cutoff frequency $f_c \approx 6.55$ GHz). The material constants and dimensions are as follows; $\varepsilon_r = 24$, $a = 9.16$ mm, $r = 0.09a$, and $w_1 = 2.5a$ (= 22.9 mm), and $w_2 = 1.8a$ (≈ 16.5 mm). In this case, single mode propagation is available between 5.93 and 9.26 GHz and between 12.33 and 17.55 GHz. Two arrays of dielectric rods are located in the corner bend of the waveguide and one pair of rods is placed at the end of the corner in the straight portion. The radius of curvature, R, is defined as the distance from the center of the circle to the center of the waveguide. If we assume that there is an integer number of dielectric rods in the 90° bend waveguide structure while maintaining a constant distance, a, between the outer dielectric rods, then

there will be the same number of inner rods as outer rods. This setup is depicted in Fig. 5(b). The reflection coefficients $|S_{11}|$ are calculated by HFSS (Ansoft Corporation, 2005). Values of $|S_{11}|$ for the case when R = 38.5 mm are shown by the dotted line in Fig. 6. Although $|S_{11}|$ are not as high as expected, they are not sufficiently small to make the waveguide practical.

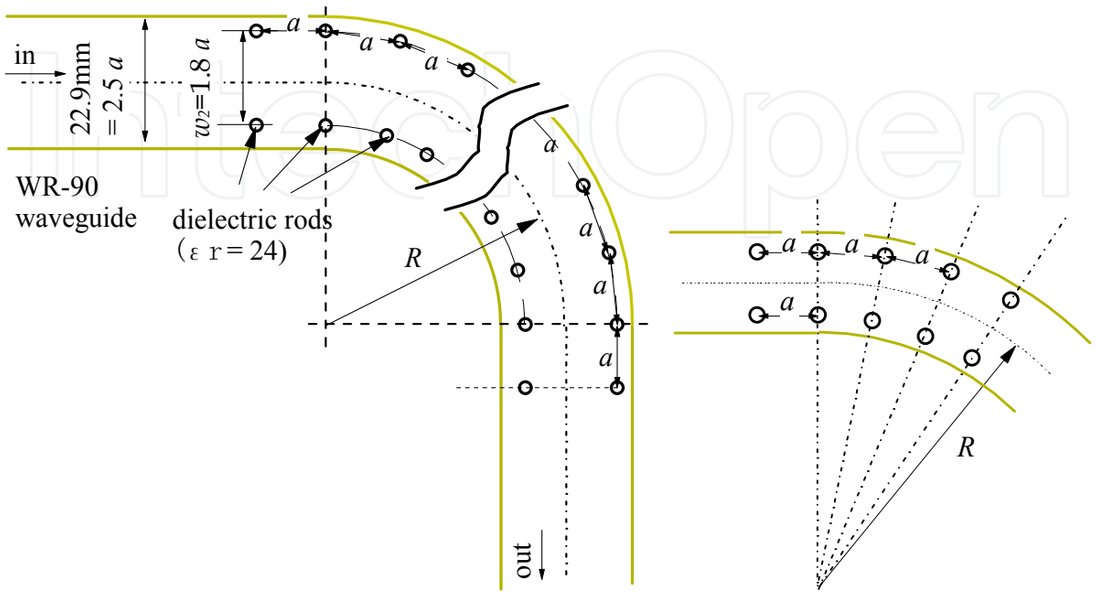

Fig. 5. (a) 90° bend waveguide with dual in-line dielectric rods. (b) Configuration of the dielectric rods in the waveguide. There is the same number of inner arrays as outer arrays.

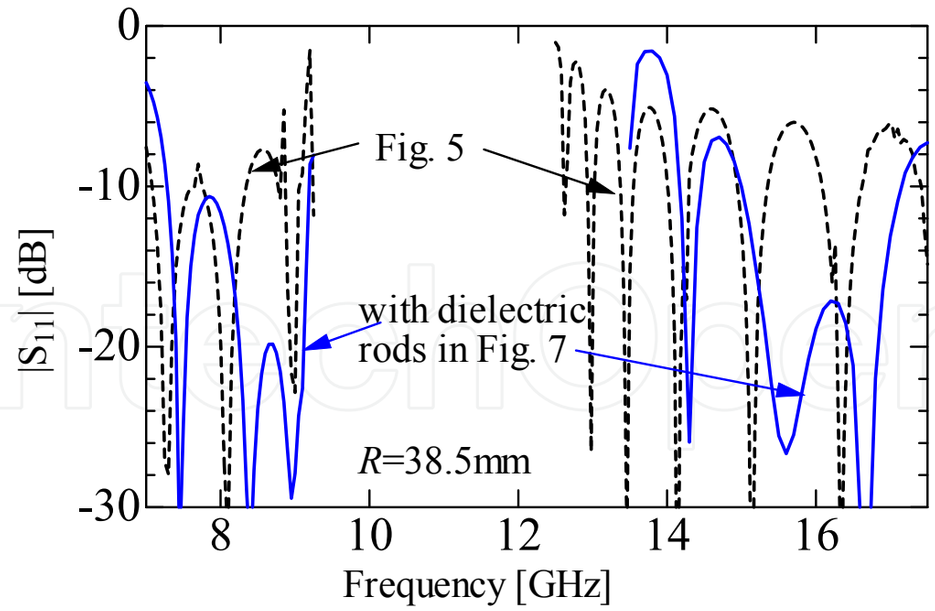

Fig. 6. Reflection coefficient $|S_{11}|$ at the corner bend of the waveguide. Solid and dotted lines denote the cases for type A and type B illustrated in Fig.9, respectively.

4. Reduction of the reflection coefficient

Other dielectric rods are set at both ends of the dielectric arrays, as shown in Fig. 7, in order to reduce the reflection $|S_{11}|$. The new dielectric rod is assumed to be Teflon. The dielectric constant and radius of the rods are ε_r = 2.08 and r = 2.85 mm, respectively. These dielectric rods function as a dielectric lens, concentrating electromagnetic waves at the center of the waveguide. The reflection coefficient calculation results for this configuration are shown by the solid line in Fig. 6.

Mode conversion may occur after passing through the corner bend, because dielectric arrays are absent in the straight waveguide portion. Only the TE_{20} mode need be considered, because the TE_{30} mode is under the cutoff condition below 19.6 GHz. The power ratio of the TE_{20} to TE_{10} electromagnetic waves is obtained. Fig. 8 shows the results for this case with new dielectric rods. The power of the TE_{20} mode is very low at frequencies higher than $2f_c$.

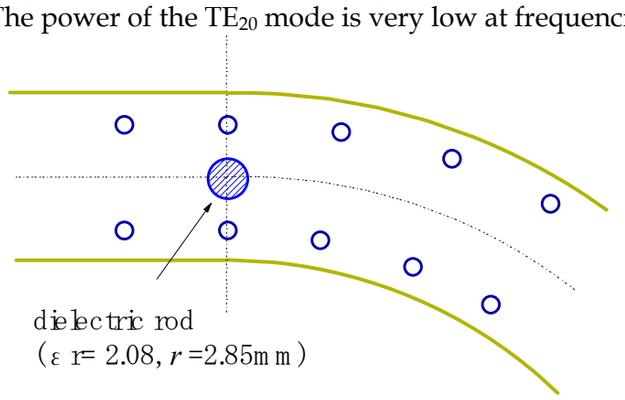

Fig. 7. Addition of another dielectric rod.

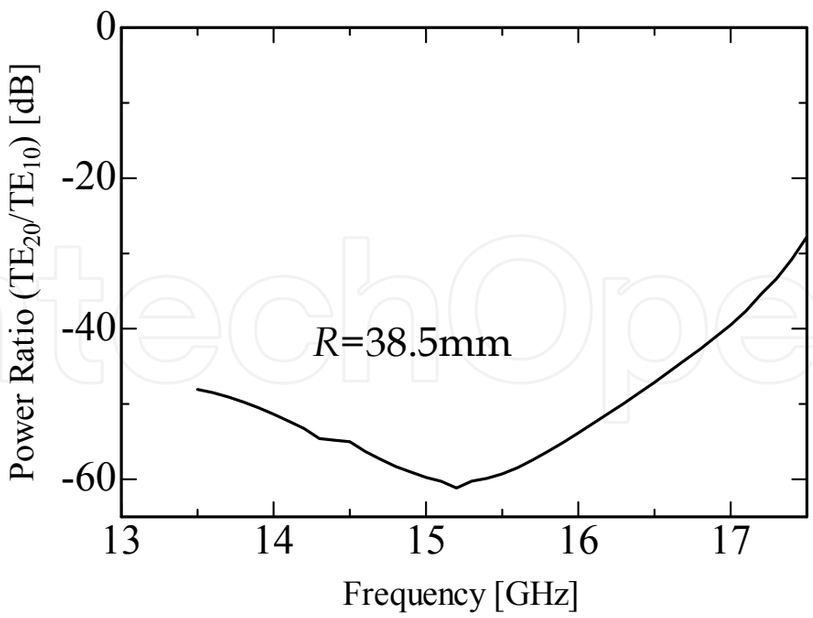

Fig. 8. Power ratio of TE_{20} to TE_{10} after passing through the waveguide.

5. Simple fabrication method

In order to fabricate of a dual-frequency band waveguide, such as the type A dual-frequency band waveguide illustrated in Fig. 9, it is necessary to locate the dielectric rods in the waveguide without a gap at the top and bottom. Such a structure may be difficult to fabricate. To overcome this problem, holes with diameters slightly larger than the rods were fabricated at the top of the waveguide and the dielectric rods were inserted into them (type B, Fig. 9). Opening a large hole in the top of the metallic waveguide, however, may be difficult since the wall current at a large hole will disturb the electromagnetic waves.
Firstly, the thick Teflon rod needs to be replaced by a thin $LaAlO_3$ rod. Fig. 10 shows an improved structure over that shown in Fig. 7. The thick dielectric rod is replaced by three $LaAlO_3$ rods having radii of 0.35 mm. The S-parameters calculated by HFSS are shown by the solid lines in Fig. 11. Secondly, S-parameters are calculated for type B in Fig. 9 with the three thin $LaAlO_3$ rods shown in Fig. 10. The diameter for inserting three thin rods is assumed to be 0.8 mm. The S-parameters calculated by HFSS are shown as dotted lines in Fig. 11. The results depicted by the solid and dotted lines are almost the same.

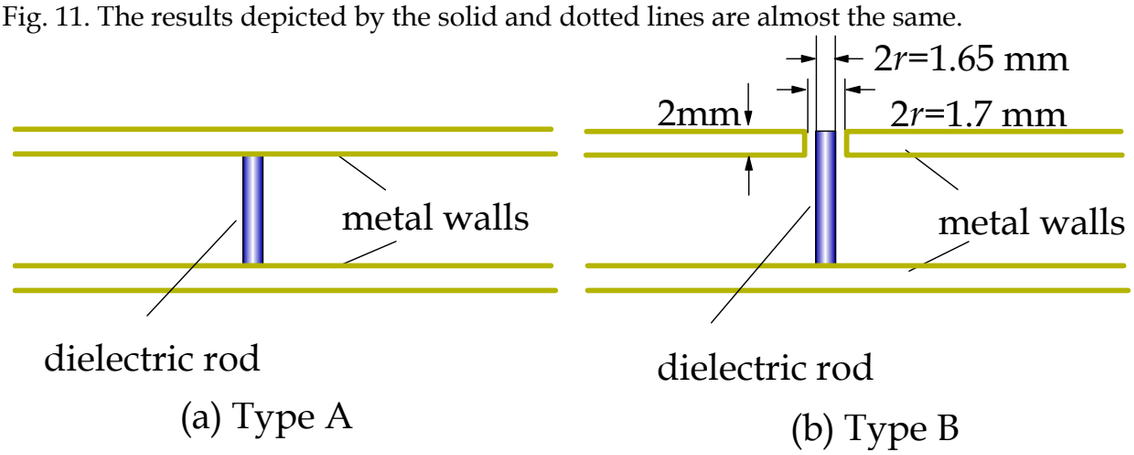

Fig. 9. (a) Dielectric rod located in a waveguide that does not have gaps at top and bottom. (b) Dielectric rod inserted in a hole made at the top of the waveguide with a diameter 0.1 mm larger than the rod diameter.

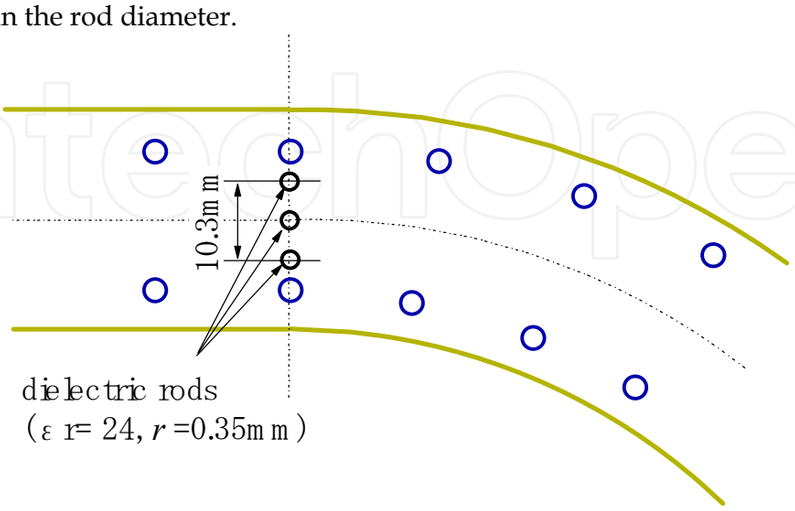

Fig. 10. Three thin $LaAlO_3$ rods that replace the thick Teflon rod shown in Fig.7

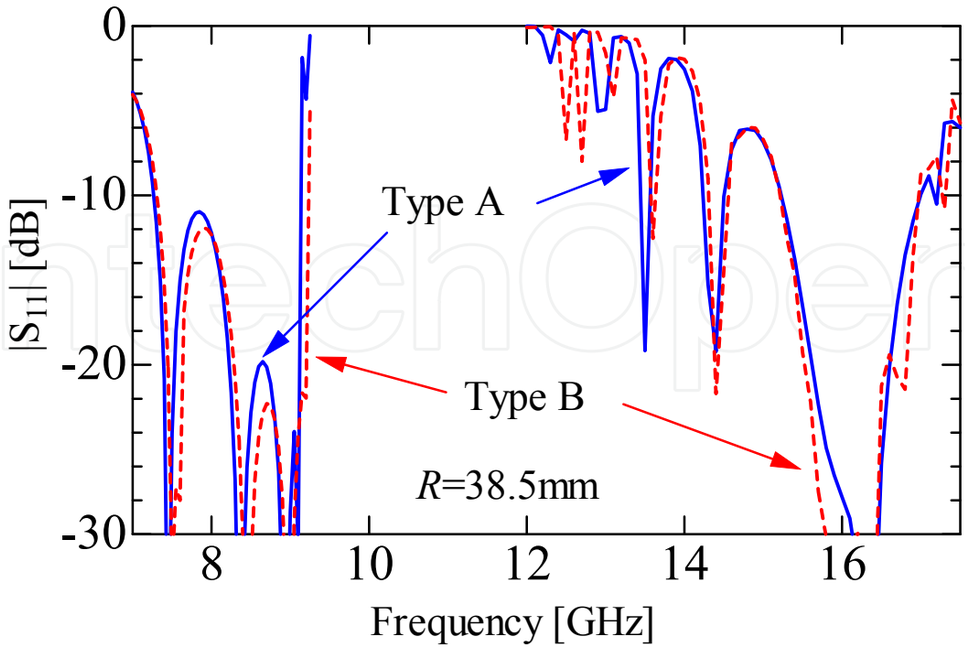

Fig. 11. Reflection coefficient $|S_{11}|$ at the corner bend of the waveguide. Solid and dotted lines denote the cases for type A and type B illustrated in Fig.9, respectively.

6. Frequency multiplexer/demultiplexer

A frequency multiplexer/demultiplexer is required to introduce electromagnetic waves into the waveguide (Kokubo & Kawai, 2008). The frequency multiplexer/demultiplexer has a height of 10.2 mm, which is same as that of a WR-90 waveguide. The basic concept of the waveguide is shown in Fig. 12. Electromagnetic waves in the low-frequency region (f_1: 5.93-9.26 GHz) propagate between ports 1 and 2, and electromagnetic waves in the high-frequency region (f_2: 12.33-17.55 GHz) pass between ports 1 and 3. Ports 1 and 2 are part of the WR-90 waveguide and port 3 is formed from a WR-62 waveguide (15.8×7.9 mm: f_c = 9.49 GHz), which is narrower than the WR-90 waveguide and is connected to the WR-90 waveguide by a tapered waveguide. Two arrays of dielectric rods are not necessary in the straight portion, because mode conversion does not occur there. We mentioned in the previous section that dielectric arrays are not necessary in the straight portion with a 90° bend waveguide. Except for two pairs of rods, all the dielectric rods were all removed from the straight portion. Accordingly, the structure of the frequency multiplexer/demultiplexer is shown in Fig. 12. Rod A, with a radius of 2.3 mm, is assumed to be made of Teflon (ε_r = 2.08) and is used to reduce the reflection. The S-parameters $|S_{11}|$ (=$|S_{22}|$) for low frequencies and $|S_{11}|$, $|S_{21}|$, $|S_{31}|$, and $|S_{33}|$ for high frequencies are calculated using HFSS. $|S_{31}|$ and $|S_{32}|$ must be zero for low frequencies, because port 3 is under the cutoff condition below 9.49 GHz and $|S_{22}|$ is not important in the high frequency region, because the design ensures that there are no high frequency components from the port 2.

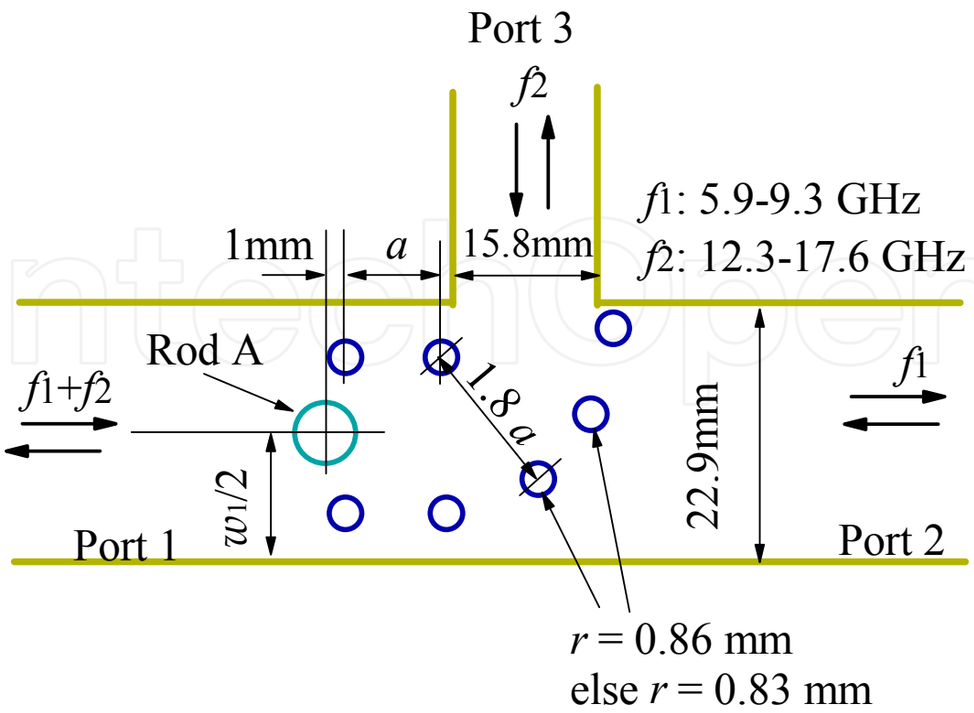

Fig. 12. Basic concept of the frequency multiplexer/demultiplexer.

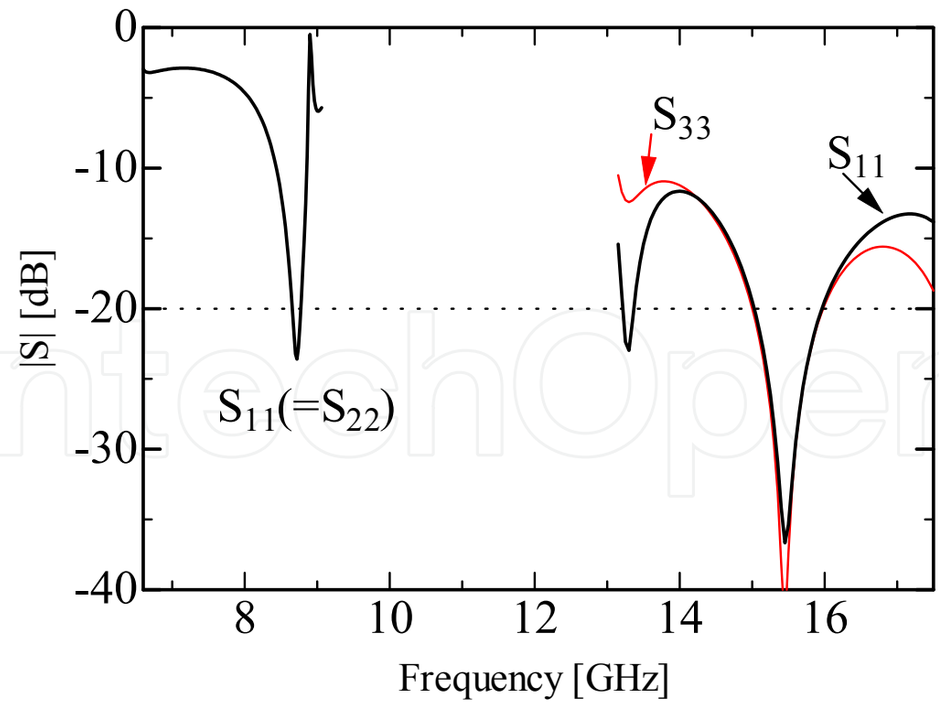

Fig. 13. Reflection coefficient $|S_{11}|$ ($=|S_{22}|$) for low frequencies and $|S_{11}|$ and $|S_{33}|$ for high frequencies.

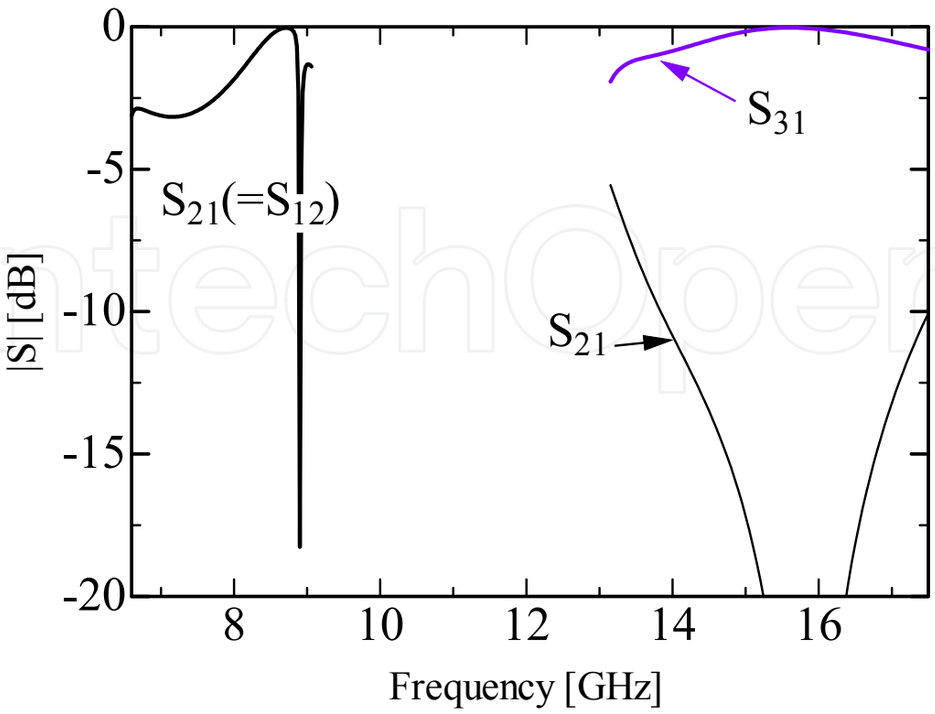

Fig. 14. $|S_{21}|$ (=$|S_{12}|$) for low frequencies and $|S_{21}|$ and $|S_{31}|$ for high frequencies.

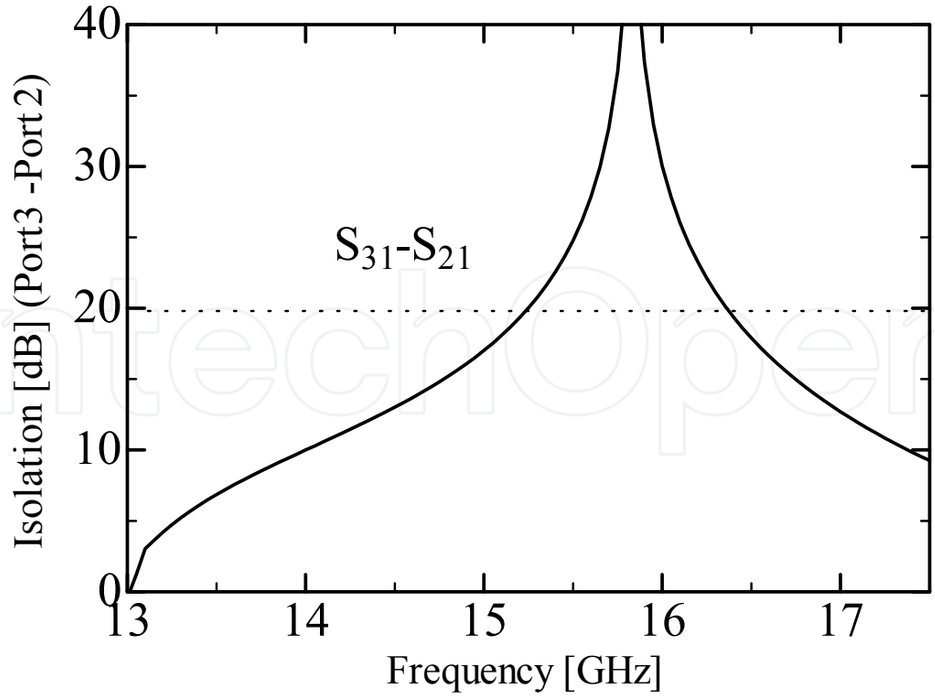

Fig. 15. Port isolation between two output ports.

The calculated results are shown in Figs. 13 and 14. If the criterion of reflection is -20 dB, then the bandwidth of $|S_{11}|$ in the low-frequency region is rather narrow. However, $|S_{21}|$ is rather small and almost all of the power from port 1 is led to port 3 at high frequencies. Port isolation between ports 2 and 3 is larger than 20 dB at frequencies between 15.3 and 16.3 GHz, as shown in Fig. 15.

7. Confirmation of mode conversion

Mode conversion of the electromagnetic waves may occur after passing through the bend from port 3 to port 1 because dielectric arrays are absent in the straight waveguide portion. Only the TE_{20} mode needs to be considered, because the TE_{30} mode is under the cutoff condition below 19.6 GHz. The power ratio of the TE_{20} to TE_{10} electromagnetic wave is obtained at port 1. The calculated results are shown in Fig. 16. Since the power of the TE_{20} mode is very low at frequencies higher than 13.1 GHz, mode conversion will not occur without dielectric rods in the straight portion.

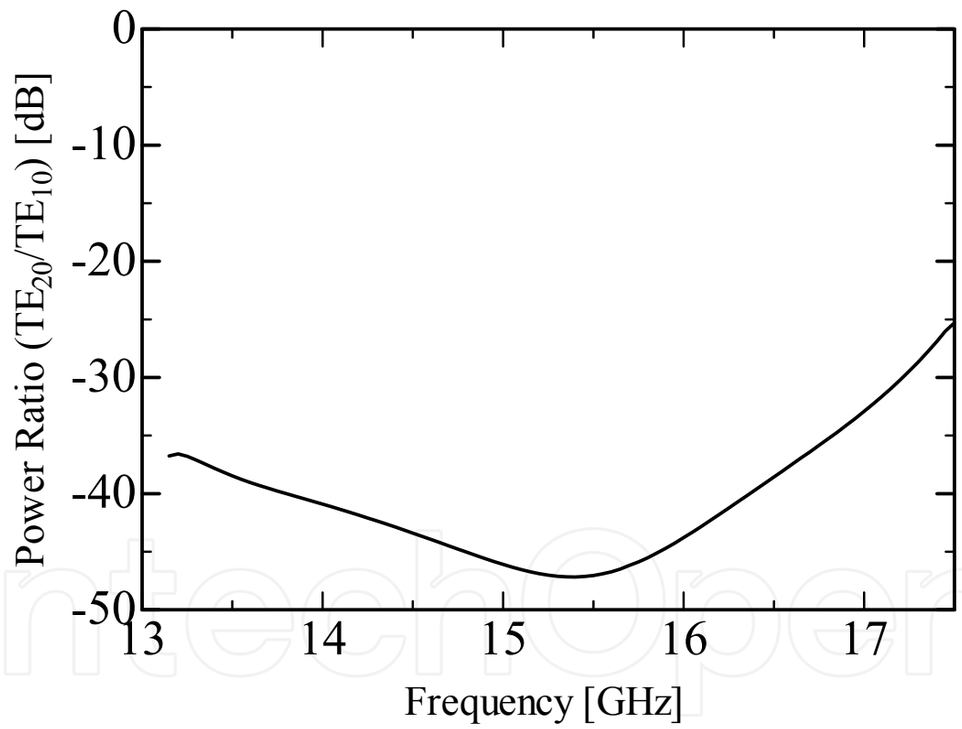

Fig. 16. Power ratio of TE_{20} to TE_{10} at port 1.

8. Simple fabrication method

As shown in the previous section, holes with diameters slightly larger than the rods will be fabricated at the top of the waveguide and the dielectric rods will be inserted (Type B, Fig. 11).

Firstly, the thick Teflon rod needs to be replaced by a thin $LaAlO_3$ rod. Fig. 17 shows an improved structure over that shown in Fig. 12. The coordinates and radii of the dielectric rods are shown in Table 1. A thick dielectric rod will be replaced by two thin $LaAlO_3$ rods having radii of 0.36 mm at separated by 7.9 mm. The S-parameters calculated by HFSS are shown by the solid lines in Figs. 18 and 19. Secondly, S-parameters are calculated for type B in Fig. 11 with two thin $LaAlO_3$ rods inserted from the top of the waveguide. The diameter for inserting three thin rods is assumed to be 0.8 mm. The S-parameters calculated by HFSS are shown by the dotted lines in Figs. 18 and 19. The results for the solid and dotted lines are almost the same. Port isolation between ports 2 and 3 is shown in Fig. 20.

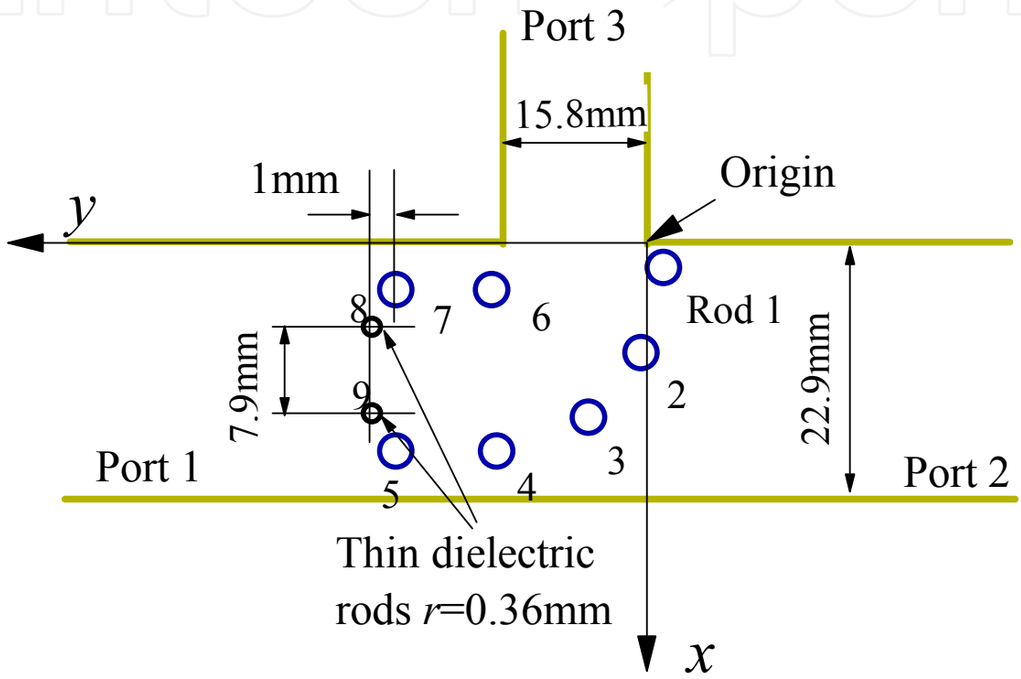

Fig. 17. Improved structure of the frequency multiplexer/demultiplexer. Two thin $LaAlO_3$ rods are used to reduce reflections.

Rod No.	Coordinate x [mm]	Coordinate y [mm]	Radius r [mm]
1	1.26	-0.29	0.83
2	10.3	1.2	0.86
3	17.1	7.3	0.86
4	19.7	16.1	0.83
5	19.7	25.2	0.83
6	3.2	16.1	0.83
7	3.2	25.2	0.83
8	7.5	26.2	0.36
9	15.4	26.2	0.36

Table 1. Coordinates and radii of dielectric rods illustrated in Fig. 17

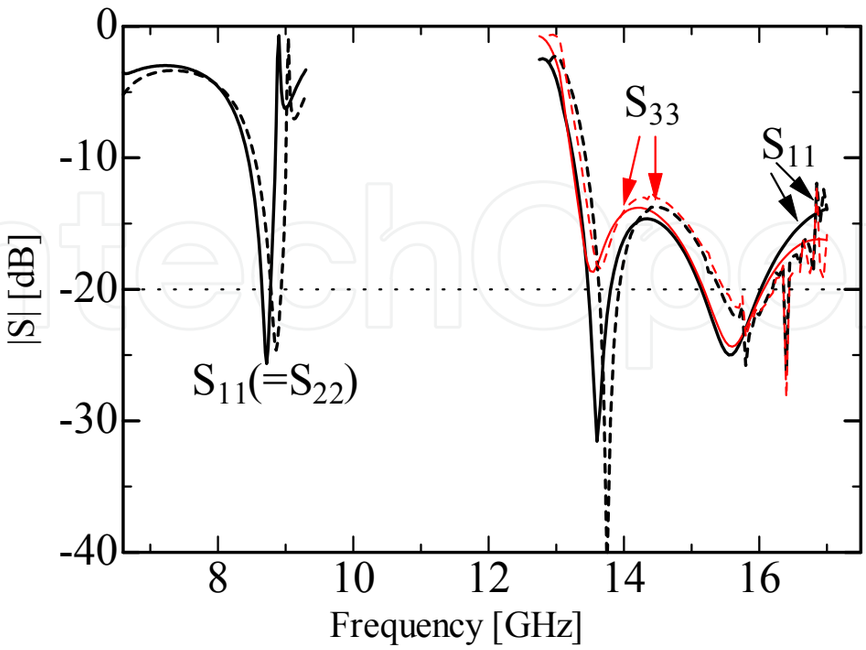

Fig. 18. Reflection coefficient $|S_{11}|$ ($=|S_{22}|$) for low frequencies and $|S_{11}|$ and $|S_{33}|$ for high frequencies. Solid and dotted lines denote the cases for type A and type B illustrated in Fig.9, respectively.

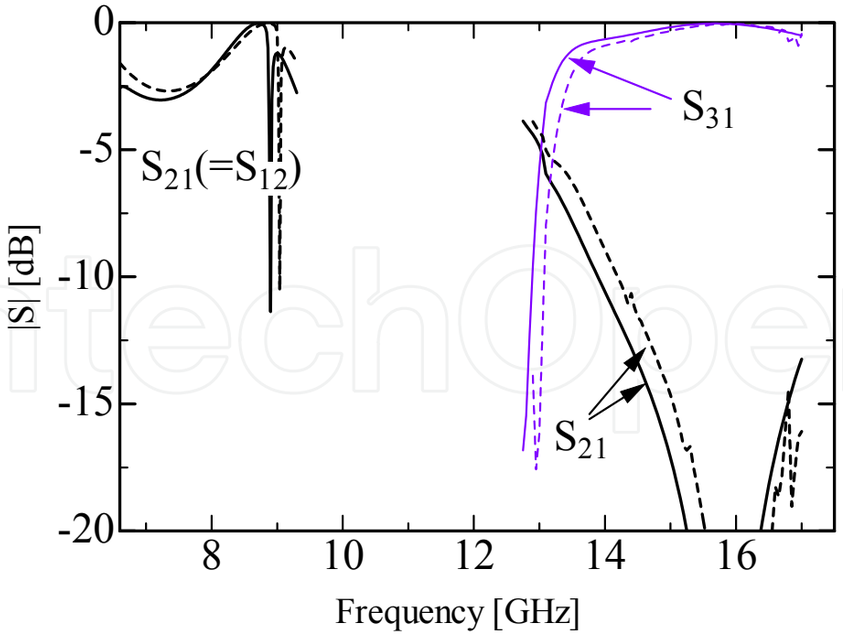

Fig. 19. $|S_{21}|$ ($=|S_{12}|$) for low frequencies and $|S_{21}|$ and $|S_{31}|$ for high frequencies. Solid and dotted lines denote the cases for type A and type B illustrated in Fig.9, respectively.

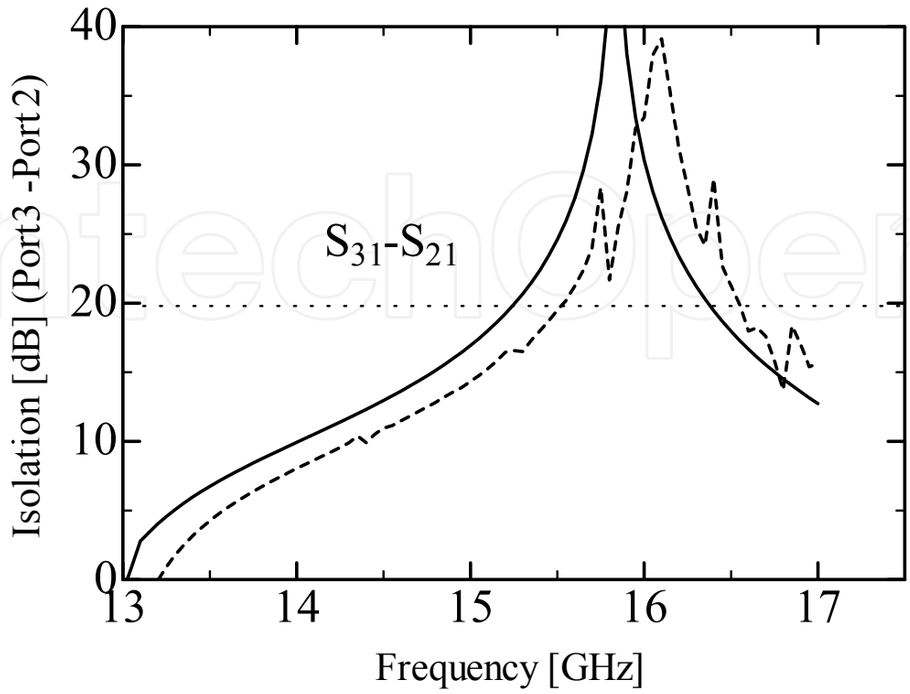

Fig. 20. Port isolation between two output ports. Solid and dotted lines denote the cases for type A and type B illustrated in Fig.9, respectively.

9. Conclusion

Electromagnetic waves were propagated in a waveguide with dual in-line dielectric rods made of $LaAlO_3$ and without higher modes above $2f_c$. Firstly, an economically feasible setup for this type of waveguide system was proposed including 90° bend waveguide. Reflection coefficients $|S_{11}|$ smaller than -18 dB were obtained at frequencies between 8.2 and 9.1 GHz and between 15.3 and 16.8 GHz by calculation. The electromagnetic wave includes less than -40 dB of the TE_{20} component in the straight portion in the case of a radius of curvature $R \geq$ 38.5 mm at frequencies below 17 GHz, so that dielectric rods are not required in the straight portion.

Secondly, a sample structure for a frequency multiplexer/demultiplexer is proposed for introducing electromagnetic waves from a coaxial cable. Reflection of electromagnetic wave occurs without dielectric rods in the straight portion; therefore, another rod, made of $LaAlO_3$ or Teflon, is introduced to reduce reflection and the calculated S-parameters. The bandwidths for reflections smaller than -20 dB are still narrow; however, optimization of the design may enable the bandwidth to be expanded.

10. References

Ansoft Corporation (2005). Introduction to the Ansoft Macro Language, HFSS v10.

Benisty, H. (1996). Modal analysis of optical guides with two-dimensional photonic band-gap boundaries, *Journal of Applied Physics*, 79, 10, (1996) pp.7483-7492, ISSN 0021-8979.

Boroditsky, M.; Coccioli, R. & Yablonovitch, E. (1998). Analysis of photonic crystals for light emitting diodes using the finite difference time domain technique, *Proceedings of SPIE*, Vol. 3283, (1998) pp.184-190, ISSN 0277-786X.

Cohn, S., B. (1947). Properties of Ridge Wave Guide, *Proceedings of the IRE*, Vol.35, (Aug. 1947) pp. 783-788, ISSN 0096-8390.

Kokubo, Y.; Maki, D. & Kawai, T. (2007a). Dual-Band Metallic Waveguide with Low Dielectric Constant Material, *37th European Microwave Conference Proceedings*, pp.890-892, ISBN 978-2-87487-000-2, Munich, Germany, Oct. 2007, EuMA, Belgium.

Kokubo, Y.; Yoshida, S. & Kawai, T. (2007b). Economic Setup for a Dual-band Metallic Waveguide with Dual In-line Dielectric Rods, *IEICE Transactions on Electronics*, Vol.E90-C, No.12, (Dec. 2007) pp.2261-2262, ISSN 0916-8524.

Kokubo, Y. & Kawai, T. (2008). A Frequency Multiplexer/Demultiplexer for Dual Frequency Waveguide, *38th European Microwave Conference Proceedings*, (Oct. 2008) pp.24-27, ISBN 978-2-87487-005-7, Amsterdam, The Netherland, Oct. 2008, EuMA, Belgium.

Maradudin, A. A. & McGurn, A. R. (1993). Photonic band structure of a truncated, two-dimensional, periodic dielectric medium, *Journal of the Optical Society of America B*, Vol.10, No.2, (1993) pp. 307-313, ISSN 0740-3224.

Shibano, T.; Maki, D. & Kokubo, Y. (2006). Dual Band Metallic Waveguide with Dual in-line Dielectric Rods, *IEICE Transactions on Electronics*, Vol.J89-C, No.10, (Oct. 2006) pp.743-744, ISSN 1345-2827 (Japanese Edition) ; Correction and supplement, ibid, Vol.J90-C, No.3, (Mar. 2007) p.298, ISSN 1345-2827. (Japanese Edition).

Tayeb, G. & Maystre, D. (1997). Rigorous theoretical study of finite-size two-dimensional photonic crystals doped by microcavities, *Journal of the Optical Society of America A*, Vol. 14, No.12, (Dec. 1997) pp. 3323-3332, ISSN 1084-7529.

Microwave and Millimeter Wave Technologies Modern UWB antennas and equipment

Edited by Igor Mini

ISBN 978-953-7619-67-1
Hard cover, 488 pages
Publisher InTech
Published online 01, March, 2010
Published in print edition March, 2010

How to reference

In order to correctly reference this scholarly work, feel free to copy and paste the following:

Yoshihiro Kokubo (2010). A Dual-Frequency Metallic Waveguide System, Microwave and Millimeter Wave Technologies Modern UWB antennas and equipment, Igor Mini (Ed.), ISBN: 978-953-7619-67-1, InTech, Available from: http://www.intechopen.com/books/microwave-and-millimeter-wave-technologies-modern-uwb-antennas-and-equipment/a-dual-frequency-metallic-waveguide-system

INTECH
open science | open minds

InTech Europe
University Campus STeP Ri
Slavka Krautzeka 83/A
51000 Rijeka, Croatia
Phone: +385 (51) 770 447
Fax: +385 (51) 686 166
www.intechopen.com

InTech China
Unit 405, Office Block, Hotel Equatorial Shanghai
No.65, Yan An Road (West), Shanghai, 200040, China
中国上海市延安西路65号上海国际贵都大饭店办公楼405单元
Phone: +86-21-62489820
Fax: +86-21-62489821

IntechOpen